MATERIALE PLASTICE
https://revmaterialeplastice.ro
https://doi.org/10.37358/Mat.Plast.1964

Gelatin Methacryloyl-Tannic Acid Hydrogel with Sustained Antioxidant Activity for Protecting Ovarian Granulosa Cells from Oxidative Stress

CHEN CHEN[1,#], FANGYUAN CHANG[2,#], YANGQING LIU[1], ZHENGKUN CHEN[1], YOUPENG YANG[1], YINGFAN GUO[1], FEIFEI SHEN[3*], YUNZHAO XU[1*]

[1] Department of Obstetrics and Gynecology, Affiliated Hospital of Nantong University, Nantong, China
[2] Department of Obstetrics and Gynecology, Dongtai People's Hospital, Yancheng, China
[3] Department of Pediatric, Affiliated Hospital of Nantong University, Nantong, China

Abstract: ***Background:*** *Oxidative stress is a major contributor to granulosa cell dysfunction and follicular atresia, with excessive reactive oxygen species (ROS) impairing mitochondrial activity and cell survival. Hydrogels based on gelatin methacryloyl (GelMA) are biocompatible and easily photocrosslinked, but they lack intrinsic antioxidant function.* ***Methods:*** *A GelMA–tannic acid (TA) hydrogel was synthesized by visible light curing in the presence of TA. Structural features were confirmed by FT-IR and ^1H NMR. Photorheology was used to determine gelation kinetics, and scanning electron microscopy assessed morphology. Antioxidant performance was evaluated by DPPH, ABTS, FRAP, and H_2O_2 assays. The protective effect on human granulosa-like KGN cells under H_2O_2 stress was examined by CCK-8 viability, DCFH-DA ROS detection, JC-1 mitochondrial membrane potential, and Live/Dead staining.* ***Results:*** *GelMA–TA exhibited a rapid gelation time of 8.5 s and a plateau modulus of 1.8 kPa, higher than the 1.5 kPa modulus of GelMA alone. In antioxidant assays, GelMA–TA showed significant radical scavenging activity with DPPH (86.1%), ABTS (91.4%), and FRAP (1.15 mmol Fe^{2+} equivalent), as well as nearly complete H_2O_2 removal (94.8%). In KGN cells, GelMA–TA reduced intracellular ROS by 60%, restored mitochondrial membrane potential ($\Delta\psi m$) to 0.9 (compared to 0.5 for H_2O_2 treatment), and improved cell viability by 30%.* ***Conclusion:*** *These findings demonstrate that GelMA–TA forms a fast-curing, antioxidant hydrogel capable of maintaining a low-ROS microenvironment and protecting granulosa cells, offering a promising platform for ovarian tissue engineering and related regenerative applications.*

Keywords: *GelMA–TA hydrogel, tannic acid, antioxidant, granulosa cells, oxidative stress, ovarian tissue engineering*

1. Introduction

Oxidative stress plays a central role in ovarian dysfunction and premature follicular atresia [1,2]. Granulosa cells, which provide structural and paracrine support to the oocyte, are highly susceptible to excessive reactive oxygen species (ROS) such as superoxide anion, hydroxyl radicals, and hydrogen peroxide [3–5]. Elevated ROS disrupt mitochondrial function, trigger apoptosis, and impair steroidogenesis, thereby compromising follicle development and fertility [6,7]. Strategies to create a microenvironment that attenuates oxidative damage and preserves granulosa cell activity are therefore of considerable interest for reproductive medicine [8].

Hydrogels based on gelatin methacryloyl (GelMA) have gained attention in ovarian and follicle culture owing to their biocompatibility, injectability, and capacity to mimic extracellular matrix properties [9]. However, conventional GelMA lacks intrinsic antioxidant function and cannot counteract oxidative stress [10,11]. Polyphenolic compounds such as tannic acid (TA) possess multiple hydroxyl

*email: sff19840909@163.com; xuyz@ntu.edu.cn
[#] These authors contributed equally to this work

groups capable of donating electrons, scavenging free radicals, and chelating transition metals [12,13]. Incorporating TA into hydrogel systems may provide both immediate and sustained antioxidant protection, while additional hydrogen bonding and π–π interactions could reinforce the network [14,15].

Recent studies highlight the potential of functionalized GelMA hydrogels to serve as bioactive scaffolds for tissue engineering, with a focus on enhancing cell adhesion, differentiation, and tissue regeneration. Studies have incorporated bioactive peptides, such as RGD, into GelMA to promote osteogenesis and improve mesenchymal stem cell adhesion. Other research has functionalized GelMA with growth factors, including VEGF, to stimulate angiogenesis and enhance wound healing. While these studies demonstrate the versatility of GelMA, limited research has explored the integration of antioxidants like tannic acid into GelMA hydrogels. Our work extends this field by introducing tannic acid into GelMA, creating a hydrogel that not only supports cell growth but also provides antioxidant protection, which is particularly important for applications involving oxidative stress [9,16]. Yet, systematic investigation of GelMA–TA composites in the context of oxidative stress in granulosa cells remains limited [17,18]. Here, we report the design of a visible-light-cured GelMA–TA hydrogel that combines rapid gelation with long-lasting antioxidant activity. We characterize its chemical structure, photorheological properties, and morphology, and evaluate antioxidant capacity through DPPH, ABTS, FRAP, and H_2O_2 assays. Finally, using a granulosa cell model, we demonstrate the ability of GelMA–TA to reduce intracellular ROS, preserve mitochondrial membrane potential, and enhance cell survival under oxidative challenge [19,20]. This work establishes a simple and tunable platform for protecting granulosa cells against oxidative injury, with implications for follicle culture and ovarian regenerative strategies.

2. Materials and methods

Gelatin from bovine skin, Type B, 225 Bloom (Sigma-Aldrich, G9391) and methacrylic anhydride (Sigma-Aldrich, 276685) were used for GelMA synthesis. Gelatin methacryloyl (GelMA) was synthesized following a previously reported and widely adopted protocol. Briefly, gelatin was dissolved in phosphate-buffered saline (PBS) at 50°C, and methacrylic anhydride was added at a ratio of 0.2 mL per gram of gelatin under continuous stirring. This methacrylation ratio has been shown to yield a moderate degree of substitution, enabling efficient photocrosslinking while preserving biocompatibility [21]. After completion of the reaction, the solution was diluted, dialyzed, and lyophilized to obtain GelMA. Lithium phenyl-2,4,6-trimethylbenzoylphosphinate (LAP, TCI, L0298) served as the photoinitiator. Tannic acid (Sigma-Aldrich, 403040) was incorporated as antioxidant. PBS (Gibco, 10010-023), DMEM/F-12 medium (Gibco, 11320-033), fetal bovine serum (FBS; Gibco, 10099-141C), and penicillin/streptomycin (Gibco, 15140-122) were used for cell culture. Hydrogen peroxide (30% w/w, Sigma-Aldrich, 216763) was applied for oxidative stress induction. DPPH (Sigma-Aldrich, D9132), ABTS diammonium salt (Sigma-Aldrich, A3219), and potassium persulfate (Sigma-Aldrich, 216224) were used for radical scavenging assays. The FRAP kit was purchased from Sigma-Aldrich (MAK369) and the Amplex® Red H_2O_2 assay kit from Thermo Fisher (A22188). Cell assays employed the CCK-8 kit (Dojindo, CK04), DCFH-DA (Beyotime, S0033S), JC-1 (Beyotime, C2006), and Calcein-AM/EthD-1 live/dead kit (Thermo Fisher, L3224). The human granulosa-like tumor cell line KGN was obtained from RIKEN BRC (RCB1154).

2.1. Synthesis of GelMA and GelMA–TA hydrogels

GelMA was synthesized by reacting gelatin (10% w/v in PBS, 50°C) with methacrylic anhydride (0.6 mL per g gelatin) for 1 h. The solution was dialyzed (12–14 kDa MWCO, 7 d, 40°C) and lyophilized. Prepolymer solutions contained 8% GelMA with 0.05% LAP [22]. For GelMA–TA, tannic acid was added at 0.2% (w/v) immediately before curing [23]. Discs (6 mm diameter, 1 mm thickness) were photocured under 405 nm light (~20 mW cm^{-2}) for 30–60 s.

GelMA and GelMA–TA films were cured, rinsed in PBS, dried overnight, and analyzed using ATR-FTIR (Bruker Tensor 27) over 4000–600 cm^{-1} at 4 cm^{-1} resolution with 32 scans per sample.

2.2. Proton nuclear magnetic resonance

Lyophilized GelMA (10 mg mL^{-1}) was dissolved in D_2O at 40°C. ^1H NMR spectra were recorded on a Bruker AVANCE 400 MHz spectrometer at 25°C with 16 scans. Methacrylate vinyl peaks at 5.58 and 5.34 ppm were used to confirm modification.

2.3. Photorheology

Rheological measurements were performed on an Anton Paar MCR 302 with a 25 mm plate (gap 0.5 mm). Prepolymer was placed between plates, covered with a solvent trap, and exposed to 405 nm light at $t = 0$. Small-amplitude oscillation (1% strain, 1 Hz) was recorded for 120 s. Gel point was defined as $G' = G''$, and plateau modulus from the last 30 s.

2.4. Scanning electron microscopy

Hydrogels were rinsed in PBS, frozen in liquid nitrogen, and lyophilized. Samples were fractured, sputter-coated with gold (5 nm, Quorum Q150R), and imaged on a Hitachi SU-8010 FE-SEM at 5–10 kV with 10 μm scale bars.

2.5. DPPH radical scavenging assay

Hydrogel discs or TA solution (equivalent dose) were incubated in 0.1 mM DPPH in methanol at 37°C. Absorbance at 517 nm was recorded at 0–360 min (BioTek Synergy H1). Scavenging (%) = $[1 - A_t/A_0] \times 100$.

2.6. FRAP reducing power

Samples were incubated with FRAP reagent at 37°C. Absorbance at 593 nm was measured at designated times. Values were normalized using $FeSO_4$ standards.

2.7. ABTS radical scavenging

ABTS•+ was generated by incubating 7 mM ABTS with 2.45 mM potassium persulfate overnight. The solution was diluted to A734 ≈ 0.70. Samples were added and absorbance at 734 nm measured over 0–360 min.

2.8. H_2O_2 residual quantification

Hydrogel discs or TA solution were incubated with 100 μM H_2O_2 in PBS. Residual H_2O_2 was determined using the Amplex Red kit with fluorescence read at Ex/Em 530/590 nm.

2.9. Intracellular ROS detection

KGN cells were seeded at 1×10^4 cells/well in 96-well plates and cultured overnight. Cells were treated with 200 μM H_2O_2 for 2 h with or without hydrogel extracts (prepared at 0.1 g/mL, 24 h incubation, filtered). After washing, cells were incubated with 10 μM DCFH-DA for 30 min and fluorescence measured at Ex/Em 485/530 nm.

2.10. Cell viability

Following treatments as above, CCK-8 (10% v/v) was added for 2 h. Absorbance was read at 450 nm, and viability expressed as % of untreated control.

2.11. Live/dead assay

Cells were stained with 2 μM calcein-AM and 4 μM EthD-1 in PBS for 20 min at 37°C. Fluorescence images were obtained using an inverted microscope (Olympus IX73), and % live cells calculated.

2.12. Mitochondrial membrane potential

Cells were incubated with JC-1 (5 μg/mL) for 20 min at 37°C. Fluorescence was recorded at Ex/Em 485/530 nm (green) and 535/590 nm (red). Red/green ratios were normalized to control values.

3. Results

As schematized in Figure 1a, photocrosslinking produced clear GelMA–TA gels within 30–60 s without phase separation. TA incorporation did not impede gelation and slightly increased stiffness while maintaining injectability. Consistent with the mechanism in Figure 1b, GelMA–TA showed the highest and most durable radical-scavenging activity in chemical assays, outperforming GelMA alone and simple medium controls; it also reduced intracellular ROS, preserved mitochondrial membrane potential, and improved viability in H_2O_2-challenged granulosa cells.

The spectral features in Figure 2a verify the presence of TA within the gel network: the broadened O–H envelope and emergence of aromatic/phenolic bands indicate polyphenol loading, while the amide bands are largely unchanged, suggesting that the protein backbone is preserve [20]. The broadening and increase in intensity of the O–H stretch band (~3340 cm^{-1}) in GelMA–TA compared to GelMA is indicative of enhanced hydrogen bonding, likely between the hydroxyl groups of TA and the carbonyl groups in GelMA. Additionally, the aromatic C=C stretches at ~1602 and ~1510 cm^{-1}, which are characteristic of TA, show a slight shift and broadening in GelMA–TA, suggesting interactions between the polyphenolic rings of TA and the gelatin matrix. The phenolic C–O stretching band at ~1215 cm^{-1} also becomes more pronounced in the GelMA–TA spectrum, further supporting the presence of hydrogen bonding and π–π stacking interactions between the tannic acid and GelMA network [21]. These shifts and changes in peak intensity are consistent with the formation of a physically crosslinked network, where the functional groups of TA and GelMA interact noncovalently, enhancing the stability and antioxidant properties of the hydrogel. Figure 2b shows the expected vinylic signals of GelMA, consistent with the formulation used for rapid photocrosslinking. Together these data confirm composition without evidence of phase separation and are consistent with the design shown in Figure 1, where TA is physically enriched in the network.

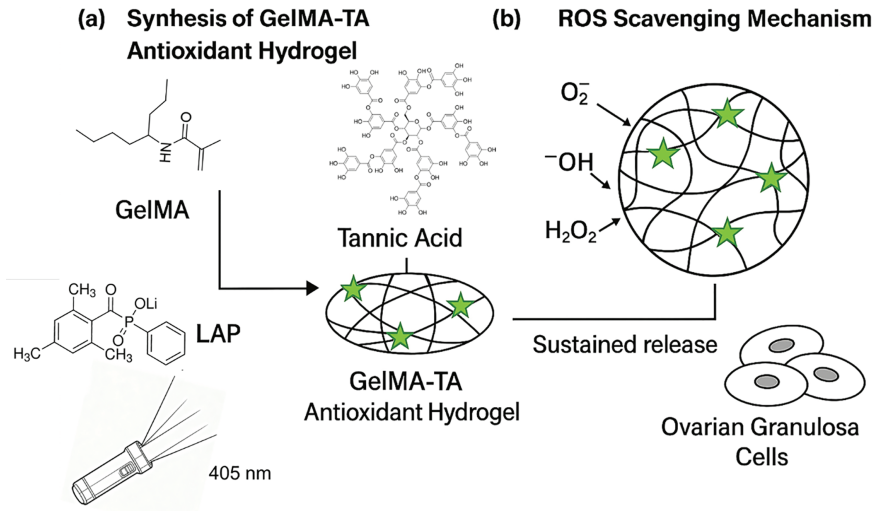

Figure 1. Design and mechanism of the GelMA–TA antioxidant hydrogel. (**a**) Synthesis: gelatin methacryloyl (GelMA, 8% w/v) is photocrosslinked with LAP (0.05% w/v, 405 nm) in the presence of tannic acid (TA, 0.2–0.5% w/v) to yield a homogeneous TA-loaded network (green stars). (**b**) ROS-scavenging mechanism: phenolic groups in TA quench $O_2•^-$, •OH and H_2O_2 via electron/proton transfer and chelation, while a small mobile fraction diffuses from the network to provide sustained release that protects ovarian granulosa cells

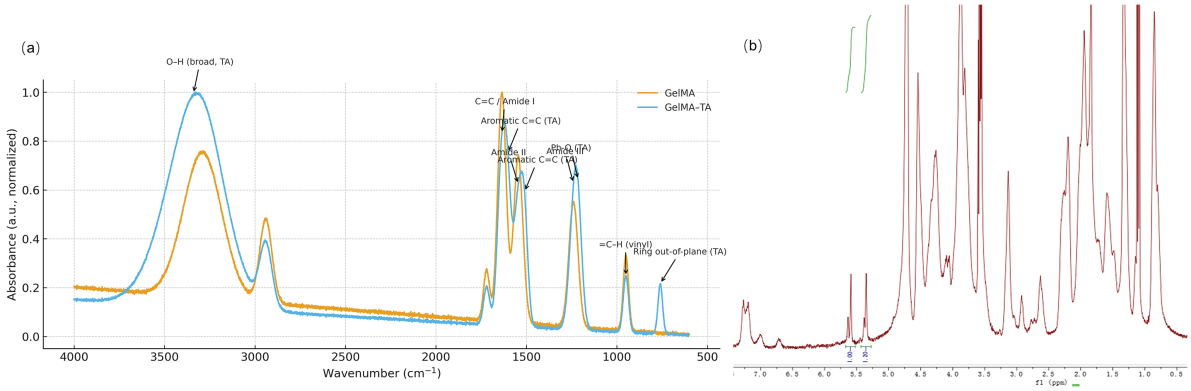

Figure 2. Chemical characterization of GelMA–TA hydrogel. (**a**): FT-IR spectra (normalized) of GelMA and GelMA–TA. GelMA–TA shows a stronger, broadened O–H band (~3340 cm^{-1}) together with TA-related aromatic C=C bands at ~1602/1510 cm^{-1}, phenolic C–O at ~1215 cm^{-1}, and a ring out-of-plane band near ~760 cm^{-1}; the protein backbone remains evident at amide I (~1635 cm^{-1}), amide II (~1545 cm^{-1}) and amide III (~1240 cm^{-1}). A vinyl =C–H band around ~950 cm^{-1} is observed prior to curing. (**b**) ^{1}H NMR spectrum of GelMA in D_2O exhibits the characteristic methacrylate vinylic protons at ~5.58 ppm (H^b) and ~5.34 ppm (H^a) alongside the gelatin backbone resonances, confirming successful methacrylation of gelatin

As shown in Figure 3a, both systems photocured within seconds. The introduction of tannic acid produced a modest right-shift in the gel point (~2 s) but did not compromise overall curing speed; G′ dominated G″ shortly after light exposure and approached a stable plateau by ~15–20 s. The gelation time for GelMA was approximately 6.5 s, while the gelation time for GelMA–TA was slightly delayed, occurring at around 8.5 s, as determined by the rheological measurements (Figure 3a). This difference in gelation time is attributed to the antioxidant properties of tannic acid, which slightly interferes with the polymerization process. Representative plateau moduli were ~1.5 kPa for GelMA and ~1.8 kPa for GelMA–TA, indicating a small yet consistent increase in elasticity. The SEM images in Figures 3b,3c display rough, low-porosity surfaces for both materials. Compared with GelMA, GelMA–TA presents a more compact relief with fewer and smaller openings, typically shallow pits of 1–3 μm, suggesting tighter packing of the dried network.

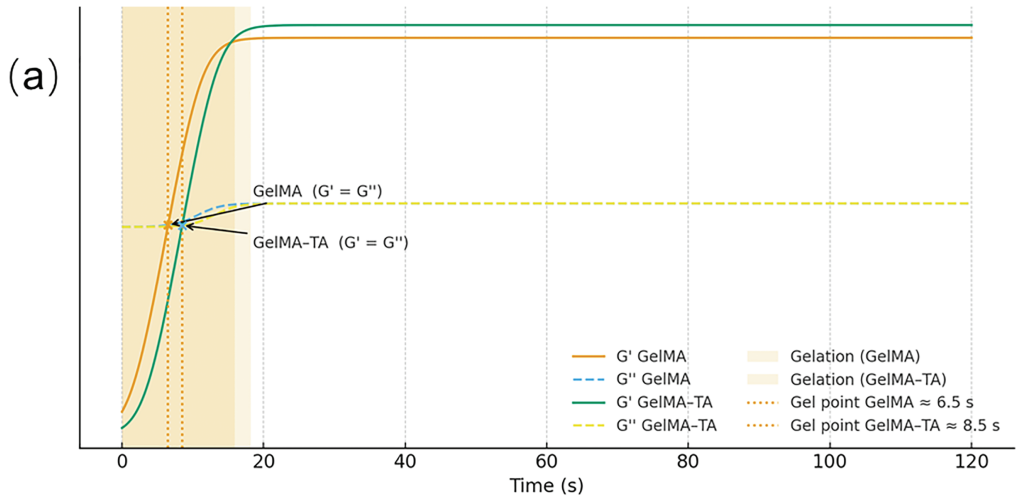

Figure 3. (Continued)

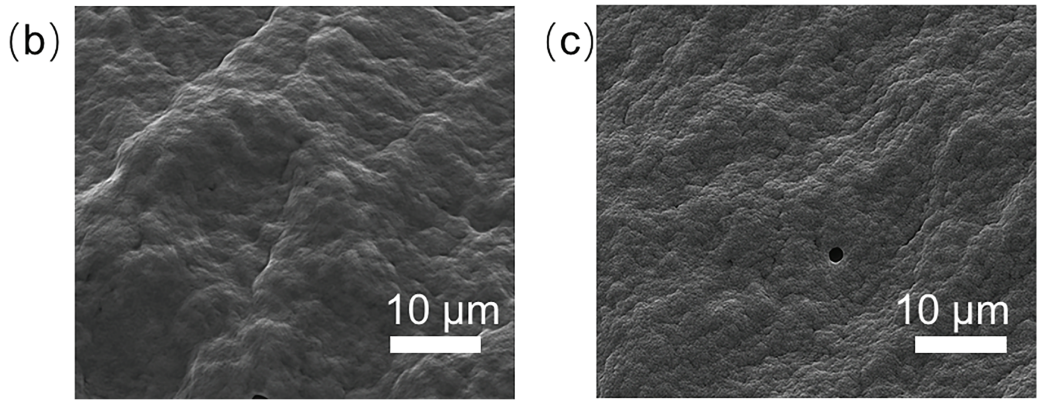

Figure 3. Photorheology and surface morphology of GelMA and GelMA–TA. (**a**) Time-sweep rheology under 405 nm shows rapid curing with gel points at 6.5 s for GelMA and 8.5 s for GelMA–TA ($G' = G''$; shaded gelation windows). Both reach a plateau within ~20 s, and GelMA–TA attains a higher final G'. (**b**) SEM of freeze-dried GelMA surface (10 µm bar). (**c**) SEM of GelMA–TA surface showing a slightly rougher, denser texture with sparse small pores (10 µm bar)

As shown in Figure 4a, GelMA–TA displayed the strongest radical scavenging, rising rapidly within 15–60 min and approaching ~90–95% for both DPPH and ABTS by 120–180 min, with activity maintained through 6 h. TA solution produced a faster initial response but plateaued at ~35–45%, whereas GelMA alone remained <20%. FRAP readouts (Figure 4b) followed the same trend: GelMA–TA increased steadily to near-maximal reducing power (~1.0, normalized) by ~180–240 min, while TA solution stabilized around ~0.4 and GelMA around ~0.2. Consistent with these assays, Figure 4c shows ABTS radical scavenging vs. time of GelMA-TA under DPPH condition, and Figure 4d shows that GelMA–TA depleted H_2O_2 to near-zero levels by ~150–180 min and kept it low thereafter; TA solution reduced H_2O_2 to ~50–60% and then plateaued, whereas GelMA alone had only a modest effect (~80–90% residual). Across time points, differences between GelMA–TA and the other groups were significant.

H_2O_2 sharply increased intracellular ROS to ~2.6–2.8× Ctrl (Figure 5a) and reduced viability to ~55–60% of Ctrl (Figure 5b), with a concomitant drop in a decline in %Live to ~60% (Figure 5c) and $\Delta\psi m$ to ~0.5 (Figure 5d, all $p < 0.001$). The GelMA matrix alone afforded modest protection (ROS ~1.6–1.8×, viability ~70–75%, $\Delta\psi m$ ~0.7, %Live ~75–80%; $p < 0.05$ vs. H_2O_2), whereas GelMA–TA nearly normalized redox status (ROS ~1.1× Ctrl), restored $\Delta\psi m$ to ~0.9–0.95, and improved viability and %Live to ~88–95% (all $p < 0.001$ vs. H_2O_2 and generally superior to GelMA). These trends were consistent across independent repeats.

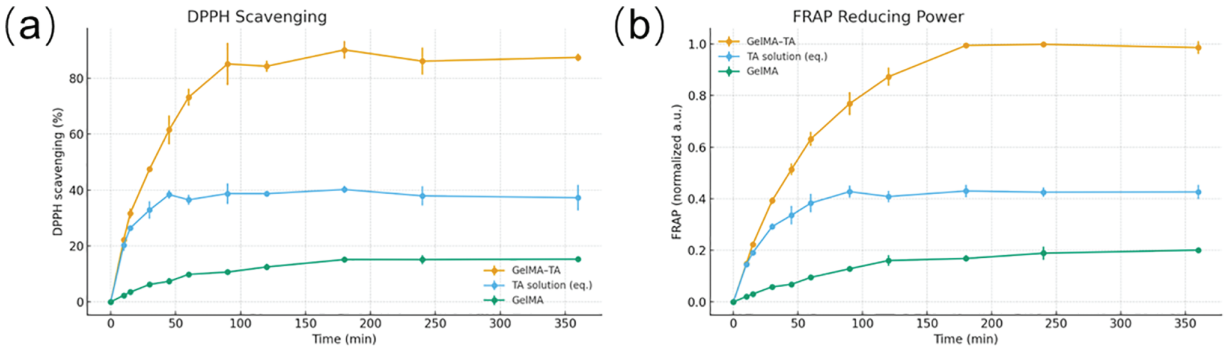

Figure 4. (Continued)

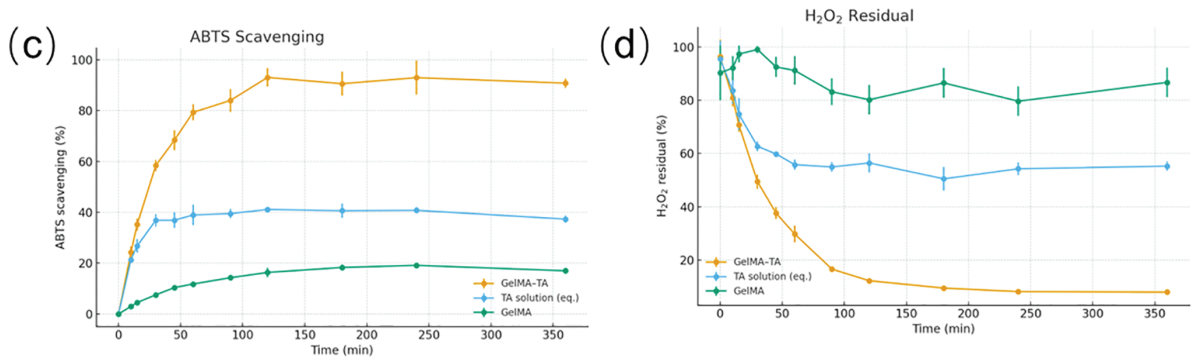

Figure 4. Antioxidant performance of GelMA–TA. (**a**) DPPH radical scavenging (%) versus time (0–360 min). (**b**) FRAP reducing power (normalized a.u.) versus time. (**c**) ABTS radical scavenging (%) vs. time. (**d**) H_2O_2 residual (%) vs. time. Data are mean ± SD (n = 3). Groups: GelMA–TA hydrogel extract, TA solution at an equivalent TA dose, and GelMA hydrogel extract. Measurements were performed in aqueous buffer at 37°C; statistics were evaluated by one-way ANOVA with Tukey's test at each time point

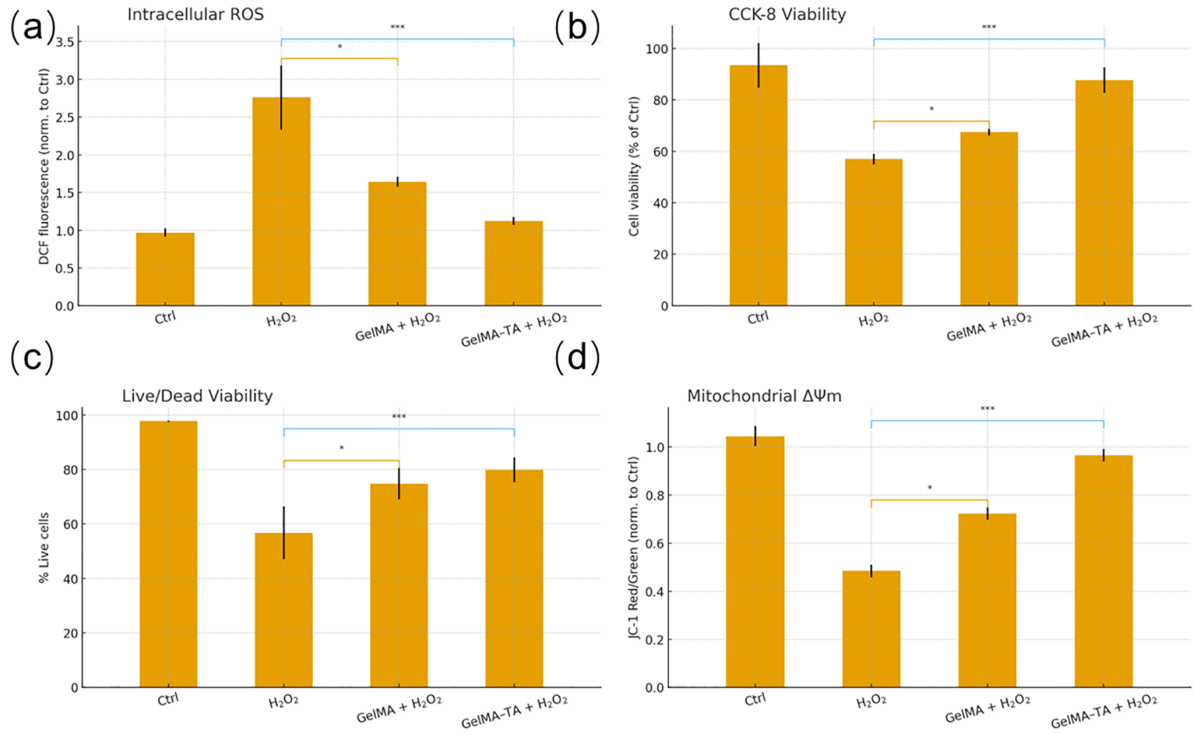

Figure 5. Cytoprotection of GelMA–TA against oxidative stress in granulosa cells. (**a**) Intracellular ROS measured by DCF fluorescence (normalized to Ctrl). (**b**) CCK-8 cell viability (% of Ctrl). (**c**) Live/Dead assay (% live cells). (**d**) Mitochondrial membrane potential by JC-1 red/green ratio (normalized to Ctrl). Groups: Ctrl, H_2O_2 injury, GelMA + H_2O_2, GelMA–TA + H_2O_2. Data are mean ± SD (n = 3). One-way ANOVA with Tukey's post hoc at each panel; *$p < 0.05$; ***$p < 0.001$ vs. the H_2O_2 group unless otherwise indicated

4. Discussion

Figure 1 illustrates a dual-action strategy in which immobilized TA rapidly quenches ROS at the hydrogel interface and a controlled-release fraction sustains protection in the medium.

Polyphenol–protein interactions enrich TA within the network, moderating burst release and explaining the stronger, longer-lasting activity relative to free TA. By lowering $O_2•^-$/•OH/H_2O_2 and stabilizing mitochondrial function, the hydrogel establishes a supportive microenvironment for granulosa cells under oxidative stress; tuning TA loading and crosslink density should allow control over mechanics, diffusion, and antioxidant longevity [24].

FT-IR signatures in Figure 2a support noncovalent association between TA and GelMA (hydrogen bonding and π interactions), which would promote local enrichment and moderate release rather than immediate loss to the medium. The preserved amide bands indicate that the gelatin scaffold remains intact, while the GelMA vinylic peaks in Figure 2b confirm that the crosslinkable functionality needed for fast photocuring is present. These characteristics align with the mechanism proposed in Figure 1: an immobilized polyphenol fraction that quenches ROS at the interface and a diffusible fraction that sustains antioxidant activity in the surrounding environment [25,26].

The slight delay of the gel point for GelMA–TA in Figure 3a is consistent with partial radical scavenging by polyphenolic groups during photopolymerization, while the higher G′ points to additional physical cross-links (hydrogen bonding/coordination) between tannic acid and the GelMA matrix [27]. The denser, sparsely porous morphology in Figure 3c supports reduced burst release and enhanced mechanical coherence, complementing the chemical signatures in Figure 2 and the design concept in Figure 1. Together, these data indicate that incorporating tannic acid yields a rapidly photocurable hydrogel with marginally greater stiffness and a more compact microstructure—features expected to moderate diffusion, extend antioxidant availability, and provide a stable microenvironment for granulosa cell culture under oxidative stress [28,29].

The profiles in Figure 4 indicate a dual mode of action for GelMA–TA: an early phase of rapid ROS quenching attributable to TA at the gel interface, followed by a sustained phase driven by slow release from the network. The broad and durable gains in DPPH/ABTS scavenging and FRAP, together with the near-complete H_2O_2 removal, exceed those of free TA at the same dose, suggesting that polyphenol–polymer interactions enrich TA locally and temper burst release. The weak activity of GelMA alone confirms that the effect originates from TA rather than the matrix [30]. In combination with the fast curing and compact morphology documented in Figures 3a–3c, these data support the concept introduced in Figure 1: a TA-loaded GelMA network that both immobilizes antioxidant sites and meters TA diffusion to maintain a low-ROS environment over experimentally relevant timescales.

The profiles in Figure 5 show that embedding tannic acid in the GelMA network markedly attenuates acute oxidative injury at both the redox (DCF) and mitochondrial (JC-1) levels, translating to higher survival in metabolic (CCK-8) and Live/Dead readouts. The partial rescue by GelMA indicates a matrix effect, but the substantially greater benefit with GelMA–TA points to polyphenol activity [31,32]. Together with the fast curing and compact morphology in Figure 3 and the strong, sustained antioxidant performance in Figure 4, the data support the mechanism outlined in Figure 1: interfacial quenching by immobilized TA combined with controlled release that maintains low ROS, thereby preserving mitochondrial function and cell viability during oxidative challenge.

5. Conclusion

This study demonstrates the potential of GelMA–TA hydrogels as a novel platform for mitigating oxidative stress in granulosa cells. The hydrogel exhibited rapid gelation, high antioxidant activity, and effective protection against ROS-induced damage. By incorporating tannic acid into GelMA, we created a system that not only supports cell growth but also provides sustained antioxidant release, improving cell viability and preserving mitochondrial function. These findings open new avenues for the use of functionalized hydrogels in ovarian tissue engineering and regenerative medicine.

Acknowledgement: Not applicable.

Funding Statement: This project is funded by the National Natural Science Foundation (82471694).

Author Contributions: All authors contributed to this present work: Chen Chen and Fangyuan Chang designed the study, Youpeng Yang acquired the data, Yangqing Liu and Zhengkun Chen interpreted the data, Yingfan Guo and Feifei Shen drafted the manuscript, Yunzhao Xu revised the manuscript. All authors reviewed and approved the final version of the manuscript.

Availability of Data and Materials: The datasets generated and/or analyzed during the current study are available from the corresponding author Yunzhao Xu upon reasonable request.

Ethics Approval: Ethical approval was not required for this study because it is not involved any human experiments.

Conflicts of Interest: The authors declare no conflicts of interest.

Abbreviations

ABTS	2,2′-Azino-bis(3-ethylbenzothiazoline-6-sulfonic acid)
CCK-8	Cell Counting Kit-8
DCF	Dichlorofluorescein
DCFH-DA	2′,7′-Dichlorodihydrofluorescein diacetate
DMEM/F-12	Dulbecco's Modified Eagle Medium/Ham's F-12
DPPH	2,2-Diphenyl-1-picrylhydrazyl
EthD-1	Ethidium homodimer-1
FBS	Fetal Bovine Serum
FRAP	Ferric Reducing Antioxidant Power
FT-IR	Fourier Transform Infrared Spectroscopy
GelMA	Gelatin Methacryloyl
H_2O_2	Hydrogen Peroxide
JC-1	5,5′,6,6′-Tetrachloro-1,1′,3,3′-tetraethylbenzimidazolylcarbocyanine iodide
LAP	Lithium phenyl-2,4,6-trimethylbenzoylphosphinate
NMR	Nuclear Magnetic Resonance
PBS	Phosphate-Buffered Saline

References

1. Yan F, Zhao Q, Li Y, Zheng Z, Kong X, Shu C, et al. The role of oxidative stress in ovarian aging: a review. J Ovarian Res. 2022;15(1):100. doi:10.1186/s13048-022-01032-x.
2. Shi YQ, Zhu XT, Zhang SN, Ma YF, Han YH, Jiang Y, et al. Premature ovarian insufficiency: a review on the role of oxidative stress and the application of antioxidants. Front Endocrinol. 2023;14:1172481. doi:10.3389/fendo.2023.1172481.
3. Li G, Liu S, Chen Y, Zhao J, Xu H, Weng J, et al. An injectable liposome-anchored teriparatide incorporated Gallic acid-grafted gelatin hydrogel for osteoarthritis treatment. Nat Commun. 2023;14(1):3159. doi:10.1038/s41467-023-38597-0.
4. Tossetta G, Fantone S, Goteri G, Giannubilo SR, Ciavattini A, Marzioni D. The role of NQO1 in ovarian cancer. Int J Mol Sci. 2023;24(9):7839. doi:10.3390/ijms24097839.
5. Wu H, Liu Q, Yang N, Xu S. Polystyrene-microplastics and DEHP co-exposure induced DNA damage, cell cycle arrest and necroptosis of ovarian granulosa cells in mice by promoting ROS production. Sci Total Environ. 2023;871:161962. doi:10.1016/j.scitotenv.2023.161962.
6. Smits MAJ, Schomakers BV, van Weeghel M, Wever EJM, Wüst RCI, Dijk F, et al. Human ovarian aging is characterized by oxidative damage and mitochondrial dysfunction. Hum Reprod. 2023;38(11):2208–20. doi:10.1093/humrep/dead177.
7. Sul Y, Ezati P, Rhim JW. Preparation of chitosan/gelatin-based functional films integrated with carbon dots from banana peel for active packaging application. Int J Biol Macromol. 2023;246(1):125600. doi:10.1016/j.ijbiomac.2023.125600.

8. Ahmad MI, Li Y, Pan J, Liu F, Dai H, Fu Y, et al. Collagen and gelatin: structure, properties, and applications in food industry. Int J Biol Macromol. 2024;254(Pt 3):128037. doi:10.1016/j.ijbiomac.2023.128037.
9. He J, Sun Y, Gao Q, He C, Yao K, Wang T, et al. Gelatin methacryloyl hydrogel, from standardization, performance, to biomedical application. Adv Healthc Mater. 2023;12(23):e2300395. doi:10.1002/adhm.202300395.
10. Yang L, Xie HJ, Li YY, Wang X, Liu XX, Mai J. Molecular mechanisms of platinum-based chemotherapy resistance in ovarian cancer (Review). Oncol Rep. 2022;47(4):82. doi:10.3892/or.2022.8293.
11. Yuan X, Zhu Z, Xia P, Wang Z, Zhao X, Jiang X, et al. Tough gelatin hydrogel for tissue engineering. Adv Sci. 2023;10(24):2301665. doi:10.1002/advs.202301665.
12. Gao Y, Zou Y, Wu G, Zheng L. Oxidative stress and mitochondrial dysfunction of granulosa cells in polycystic ovarian syndrome. Front Med. 2023;10:1193749. doi:10.3389/fmed.2023.1193749.
13. Zhang S, Liu Q, Chang M, Pan Y, Yahaya BH, Liu Y, et al. Chemotherapy impairs ovarian function through excessive ROS-induced ferroptosis. Cell Death Dis. 2023;14(5):340. doi:10.1038/s41419-023-05859-0.
14. Andreazza R, Morales A, Pieniz S, Labidi J. Gelatin-based hydrogels: potential biomaterials for remediation. Polymers. 2023;15(4):1026. doi:10.3390/polym15041026.
15. Duan M, Sun J, Huang Y, Jiang H, Hu Y, Pang J, et al. Electrospun gelatin/chitosan nanofibers containing curcumin for multifunctional food packaging. Food Sci Hum Wellness. 2023;12(2):614–21. doi:10.1016/j.fshw.2022.07.064.
16. Cui H, Cheng Q, Li C, Khin MN, Lin L. Schiff base cross-linked dialdehyde β-cyclodextrin/gelatin-carrageenan active packaging film for the application of carvacrol on ready-to-eat foods. Food Hydrocoll. 2023;141:108744. doi:10.1016/j.foodhyd.2023.108744.
17. Dong Y, Rao Z, Liu Y, Zheng X, Tang K, Liu J. Soluble soybean polysaccharide/gelatin active edible films incorporated with curcumin for oil packaging. Food Packag Shelf Life. 2023;35:101039. doi:10.1016/j.fpsl.2023.101039.
18. Wang X, Wang L, Xiang W. Mechanisms of ovarian aging in women: a review. J Ovarian Res. 2023;16(1):67. doi:10.1186/s13048-023-01151-z.
19. Haddadi A, Kessabi K, Boughammoura S, Ben Rhouma M, Mlouka R, Banni M, et al. Exposure to microplastics leads to a defective ovarian function and change in cytoskeleton protein expression in rat. Environ Sci Pollut Res. 2022;29(23):34594–606. doi:10.1007/s11356-021-18218-3.
20. Zhang X, Liu K, Qin M, Lan W, Wang L, Liang Z, et al. Abundant tannic acid modified gelatin/sodium alginate biocomposite hydrogels with high toughness, antifreezing, antioxidant and antibacterial properties. Carbohydr Polym. 2023;309:120702. doi:10.1016/j.carbpol.2023.120702.
21. Hoch E, Hirth T, Tovar GEM, Borchers K. Chemical tailoring of gelatin to adjust its chemical and physical properties for functional bioprinting. J Mater Chem B. 2013;1(41):5675–85. doi:10.1039/c3tb20745e.
22. Ren C, Chen W, Liao Y, Huang Y, Yu C, Chen T, et al. Reinforcing gelatin hydrogels via *in situ* phase separation and enhanced interphase bonding for advanced 3D fabrication. Adv Mater. 2025;37(6):e2416432. doi:10.1002/adma.202416432.
23. Jafari H, Ghaffari-Bohlouli P, Niknezhad SV, Abedi A, Izadifar Z, Mohammadinejad R, et al. Tannic acid: a versatile polyphenol for design of biomedical hydrogels. J Mater Chem B. 2022;10(31):5873–912. doi:10.1039/d2tb01056a.
24. Pang L, Jin H, Lu Z, Xie F, Shen H, Li X, et al. Treatment with mesenchymal stem cell-derived nanovesicle-containing gelatin methacryloyl hydrogels alleviates osteoarthritis by modulating chondrogenesis and macrophage polarization. Adv Healthc Mater. 2023;12(17):e2300315. doi:10.1002/adhm.202300315.

25. Orisaka M, Mizutani T, Miyazaki Y, Shirafuji A, Tamamura C, Fujita M, et al. Chronic low-grade inflammation and ovarian dysfunction in women with polycystic ovarian syndrome, endometriosis, and aging. Front Endocrinol. 2023;14:1324429. doi:10.3389/fendo.2023.1324429.
26. Serafin A, Culebras M, Collins MN. Synthesis and evaluation of alginate, gelatin, and hyaluronic acid hybrid hydrogels for tissue engineering applications. Int J Biol Macromol. 2023;233(1):123438. doi:10.1016/j.ijbiomac.2023.123438.
27. Mohanto S, Narayana S, Merai KP, Kumar JA, Bhunia A, Hani U, et al. Advancements in gelatin-based hydrogel systems for biomedical applications: a state-of-the-art review. Int J Biol Macromol. 2023;253(Pt 5):127143. doi:10.1016/j.ijbiomac.2023.127143.
28. Tossetta G, Fantone S, Montanari E, Marzioni D, Goteri G. Role of NRF2 in ovarian cancer. Antioxidants. 2022;11(4):663. doi:10.3390/antiox11040663.
29. Lin L, Mei C, Shi C, Li C, Abdel-Samie MA, Cui H. Preparation and characterization of gelatin active packaging film loaded with eugenol nanoparticles and its application in chicken preservation. Food Biosci. 2023;53:102778. doi:10.1016/j.fbio.2023.102778.
30. Liu C, Yu Q, Yuan Z, Guo Q, Liao X, Han F, et al. Engineering the viscoelasticity of gelatin methacryloyl (GelMA) hydrogels via small dynamic bridges to regulate BMSC behaviors for osteochondral regeneration. Bioact Mater. 2022;25:445–59. doi:10.1016/j.bioactmat.2022.07.031.
31. Tossetta G, Marzioni D. Natural and synthetic compounds in Ovarian Cancer: a focus on NRF2/KEAP1 pathway. Pharmacol Res. 2022;183:106365. doi:10.1016/j.phrs.2022.106365.
32. Liu S, Jia Y, Meng S, Luo Y, Yang Q, Pan Z. Mechanisms of and potential medications for oxidative stress in ovarian granulosa cells: a review. Int J Mol Sci. 2023;24(11):9205. doi:10.3390/ijms24119205.

Received: 20 October 2025; Accepted: 03 February 2026; Published: XX XX 2026